Imperial College
London

Final report for MSc Project

Improving arrhythmias detection by complementing existing electrical sensors with additional sensors

Author name

Christos Dolopikos Supervisor(s):

Dr. Zachary Whinnett

Dr. Matthew Shun-Shin

Submitted in partial fulfilment of the requirements for the award of MSc in Biomedical Engineering from Imperial College London

September 2020

Word count: 5971

Abstract

The aim of the project is the implementation of a laser Doppler sensor on an Implantable Cardioverter Defibrillator (ICD) to reduce the amount of inappropriate shocks. In this work Electrocardiogram (ECG) and Photoplethysmography (PPG) data from 252 patients was collected. The data were cleaned from noise artifacts using a low and high pass filter and a sliding average window, respectively. Afterwards, extraction of statistical features from both signals occurs on a beat-by-beat basis. During this process a new bio-marker is introduced, perfusion discriminant to determine the how critical the condition of a patient is. A random forest classifier is incorporated for classifying the condition of the patient as Normal, Noise, Simulated VT, Simulated SVT, and Clinical VT with 83.20%. Cases classified as Simulated VT, Simulated SVT, and Clinical VT would be further examined by another random forest classifier as Shock or No-Shock instances. The suggested treatment of the latter random forest is combined with a rule based decision-making mechanism, that achieved accuracy levels of 97.46% on the fly. Decreasing inappropriate treatments from 18.5% (conventional ICDs) to 1%, successfully providing proof of concept.

Acknowledgements

I would like to express my thankfulness to my family and friends for their continuous support and encouragement throughout my life.

My deepest appreciation to Dr. Zachary Whinnett for giving the opportunity to work on this project and be part of his research.

I would also like to express my deep gratitude to Dr. Matthew Shun-Shin and Dr. Alejandra Miyazawa for making me feel as part of the team but most importantly for their constant mentoring and support.

Table of Contents

1. Introduction

Cardiovascular disease is now the leading causes of death worldwide (World Health Organization, 2018). Patients with known cardiac disease, such as severe heart failure or an inherited cardiac condition and are at risk of sudden cardiac death may receive an Implantable Cardioverter Defibrillator (ICD). ICDs are small (53.71mm x 73.6mm x 1.0mm, 29.5 cm^3, 69g)(Peyrol *et al.*, 2017) devices with one or more leads that go into or around the heart to both sense for rhythm disturbances and deliver a shock or other electrical therapy to restore a normal heart rhythm. Across multiple randomised controlled trials, ICDs have been found to reduce sudden cardiac death caused.

However, ICDs are not without risk. In addition to the inherent risks associated with an having a permanent implantable device (such as infection, bleeding, and lead migration) they can also fail in two ways. Firstly, they may deliver a shock or therapy when it is not clinically required. This may occur when the patient is completely well and without a ventricular arrhythmia. The device has mis-interpreted the electrical activity (perhaps because of a lead fracture causing noise on a wire, or because of a benign atrial tachycardia) as showing a dangerous ventricular arrhythmia. This is termed an inappropriate shock. It may also correctly detect potentially dangerous electrical activity, while the patient is tolerating it. Thus, the device would deliver appropriate, but unnecessary therapy. This is called an unnecessary shock. Alternatively, the device may consider electrical activity as normal when it is in-fact dangerous and withhold a shock. This may occur during episodes of "slow ventricular tachycardia (VT)".

Whilst appropriate and necessary shocks are lifesaving, recent data finds that inappropriate and unnecessary shocks are harmful and lead to higher mortality (Van Rees *et al.*, 2011). Furthermore, it is estimated that 18% of shocks are inappropriate. In addition to the increased mortality, these shocks can damage the heart and traumatise a patient.

In order to reduce inappropriate therapies, current programming guidelines recommend an increased heart rate threshold and delaying treatment. This, however, may lead to ICDs either not delivering or delaying treatment to slower, haemodynamically compromising VTs.

The fundamental limitation of existing ICDs is that they only have electrical information available to them. The addition of haemodynamic or tissue perfusion data could fundamentally change how they work and improve lives.

This project aims to determine how tissue perfusion data, using a miniaturized laser Doppler sensor, could potentially be added to an ICD to improve its decision-making algorithm.

1.1. The Heart

The heart is comprised of four chambers, two atria (upper left and right chambers) and two ventricles (lower left and right chambers). Upper and lower chambers are separated by atrioventricular (AV) valves, which ensure a unidirectional blood flow from an atrium to its corresponding ventricle. The atria are responsible for controlling the inflow of blood to the heart (both oxygenated and non-oxygenated blood), whereas the ventricles' main function is related to the outflow (pumping) of the blood away from the heart to the rest of the body. The rate under which these chambers contract is defined by the sino-atrial node also known as the heart's natural pacemaker. The sinus node generates an electrical stimulus that initiates the contraction of the right atrium.

The electrical impulse propagates through the right atrial myocardium by generating an action potential (AP) reaching the AV node. The AV node consists out of a set of cells that are the only path for the AP to propagate from the atria to the ventricles. To avoid an instant contraction of the ventricle, the AV node delays the propagation of the signal allowing enough time for a volumetric shift to occur. When blood volume within the ventricle is greater than that in the atrium due to the pressure difference of the chambers the AV valves close. Simultaneously, the propagation of the electrical signal to the ventricular myocardium results in the contraction of the ventricle(Ward,Jeremy P. T. ; Linden, 2017). This process describes a normal heart rhythm, which when disrupted causes an arrhythmia (Figure 1). An arrhythmia describes an altered heart rhythm.

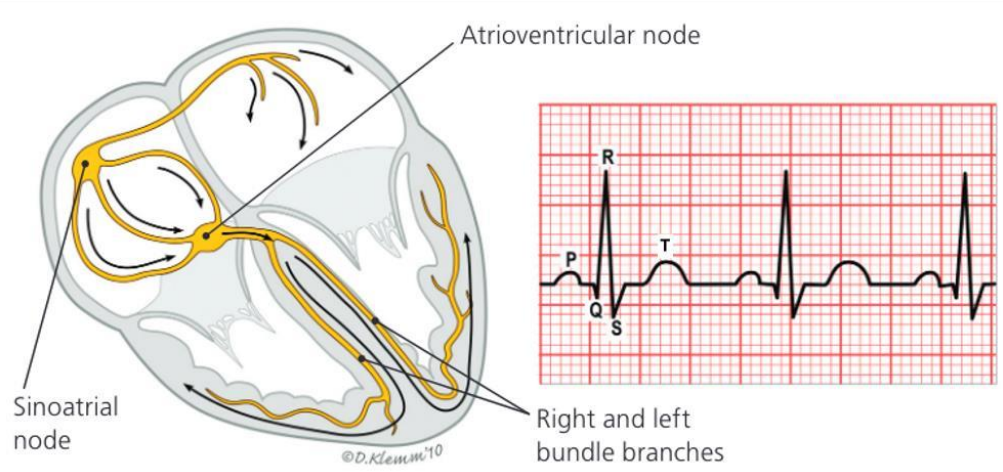

Figure 1: Normal Sinus rhythm and Electrocardiogram(Helton, 2015)

Rapid rhythm generated from the ventricles of the heart is characterised as VT. It affects the pumping function of the cardiac muscle which usually results in high rates of beats per minute (150-200 BPM). In the case of severe rapid VT, the heart fails to pump blood effectively to the rest of the body. Loss of cerebral perfusion may result in loss of consciousness of the patient or for prolonged periods, this might be terminal(Johns Hopkins Medicine, 2020).

When incoordinate electrical signals reach the ventricular myocardium, quiver ventricular contractions occur. This phenomenon is known as Ventricular Fibrillation (VF)(Medicine, 2020). Despite the high metabolic rate of the muscle inefficient production of contractions is generated(Wiggers, 1940). Therefore, blood outflow is insufficient leading to a significant drop in arterial pressure resulting in loss of consciousness. Due to low oxygenation of the brain and spinal cord, ineffective breathing occurs until asphyxia takes place and death results within six to eight minutes. Current ICDs do not give therapy for all arrhythmias, only those that it suspects pose a life-threatening condition.

1.2. Electrocardiogram (ECG)

An ECG measures the bio-electrical activity of the heartbeat. Each heartbeat is represented by a signal wave depending on the phase of the cardiac cycle (Davey & Sharman, 2018).

As previously discussed, the cycle starts at the Sinoatrial node and the AP propagates across the atrial myocardium resulting in atrial repolarization. This is translated to an ECG by a small deflection of the signal causing a wave, called a P-wave. Transmission of the AP through the AV node to the ventricles causes the ventricles to depolarize, creating the QRS complex on an ECG. QRS represents the contraction of the ventricle which allows the circulation of blood to either the lungs or the rest of the body. After the contraction of the ventricular cardiac muscle, the muscle relaxes and starts to repolarize. This repolarization process is depicted as a T-wave on an ECG. (Ward,Jeremy P. T. ; Linden, 2017)

To record such a signal, electrodes are placed on the human body recording the action potentials of the cardiac muscles.

1.3. Laser Doppler Flowmetry (LDF)

In general, the Doppler phenomenon is exploited in a variety of medical applications. Laser Doppler flowmetry (LDF) is the utilization of the Doppler phenomenon to measure changes in blood velocity. It is a non-invasive method and therefore can be incorporated into an ICD without requiring any additional leads/ electrodes entering the cardiac muscle.

The main components of a LDF are a transducer and a receiver. These two are located closely to each other and are placed on the blood vessel wall. When attached on the blood vessel it is then possible to extract features of clinical importance.

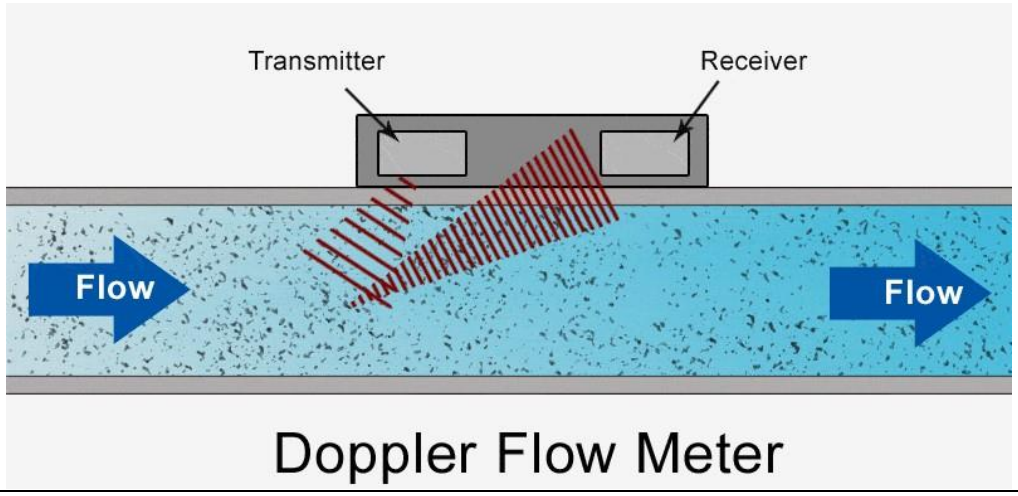

Figure 2: Laser Doppler flowmeter set up(Patrick Mullins, 2016)

The transducer emits a signal/ laser of a predefined frequency which will then is going to be reflected to the transducer/ receiver. The reflection occurs either because the signal reached the blood vessel wall on the opposite cite or because an obstacle intersected with it. If the signal meets an obstacle before hitting the opposite blood vessel wall, then it is going to return faster to the receiver and therefore will have an altered frequency. In blood vessels such obstacles are created by red blood cells. During systole (heart contraction) the velocity of the red blood cells increases, and areas of high red blood cell concentration are created, whereas during diastole (heart relaxation) there are less concentrated areas. Therefore, during diastole, the predefined emitted frequency is not going to massively deviate from the reflected and then received frequency. In contrary high concentration areas will create a cloud effect which will pose as an obstacle for the signal to reach its opposite wall, significantly altering the received frequency(Tamura, 2014).

The change of frequency can be used to estimate the velocity of the red blood cells and therefore estimate the blood flow.

$$f_0 = \frac{v + v_0}{v + v_s} f_s \quad (1)$$

Where f_0 is the observer frequency (received), f_s is the actual frequency transmitted, $v_0$is the observer's velocity (received) and $v_s$is the source velocity (emitted), and v is the velocity of the laser, Figure 2.

The exact device used in this project is a Photoplethysmography (PPG) sensor, that operates under the same principals with as an LDF. This could be an important addition to ICDs as PPG data can be used to determine peripheral perfusion. For instance, under normal circumstances an adequate perfusion is anticipated whereas during VT, a less adequate perfusion is expected.

1.4. Implantable Cardioverter-Defibrillator (ICD)

An ICD (Figure 3) is a cardiac implantable electronic device that prevents sudden cardiac death (SCD) caused by ventricular arrhythmias. The components of an ICD are a pulse generator, at least one lead wire (max. three), electrodes (located at the tip of the wire), and a battery (Thompson-Nauman,Amy E. ; Christie,Melissa G.T. ; Degroot,Paul J. ; Dolan, 2014). The electrodes can be placed either within the heart itself or in great proximity to the heart allowing for the electrical pulse to reach the cardiac muscle. When a ventricular arrhythmia is detected, the ICD may send a high-energy electrical pulse (shock) or set of pulses (Antitachycardia pacing (ATP)) to restore the cardiac rhythm. VF, without therapy, results in death within a couple of minutes. VT may be similarly poorly tolerated. However, often patients after a few seconds or tens of seconds may spontaneously cardiovert. Furthermore, whilst there is clear cardiac limitation, overall, their condition may be tolerated for minutes to hours. Nevertheless, as ICDs do not have access to perfusion or clinical data, all rhythms are rapidly treated with electrical therapy.

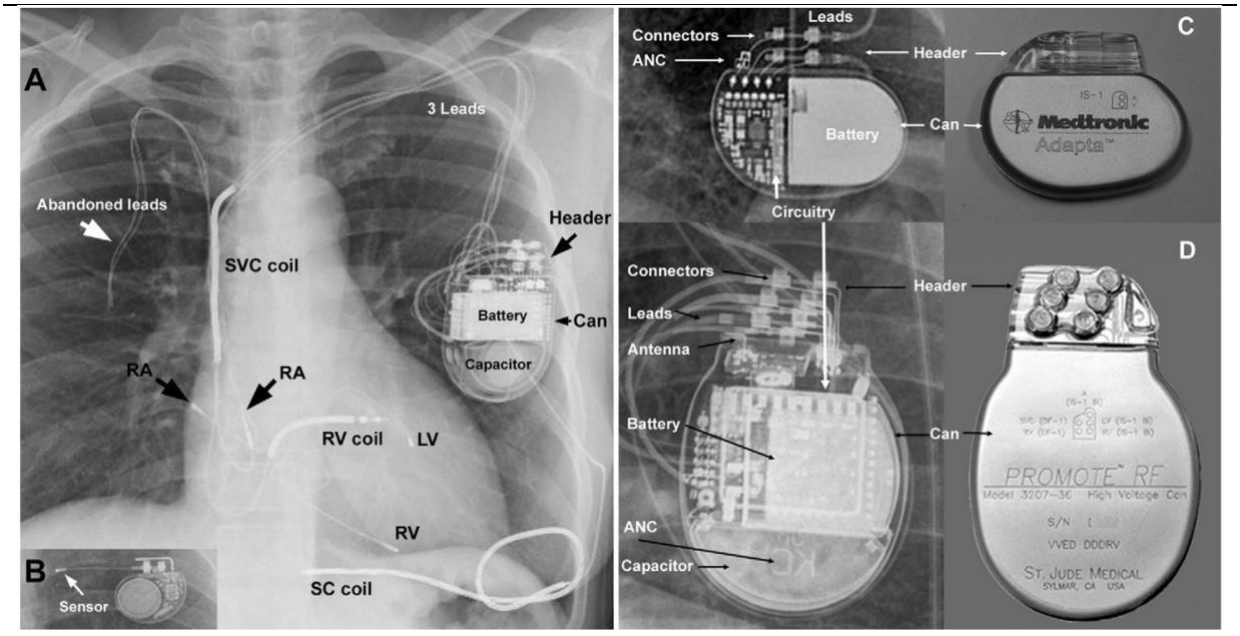

Figure 3: (A) Chest X-ray of patient with ICD. (B) Sensor of cardiac activity. (C) Detailed diagram component. (Aguilera, Volokhina & Fisher, 2011)

The effectiveness of an ICD depends on its ability to detect fatal ventricular arrhythmias. Due to the complexity of the cardiac cycle, it is common for arrhythmia detection algorithms to misjudge a patient's conditions and register inappropriate shocks. A shock treatment is considered as inappropriate when it is delivered in the absence of a life-threatening condition, like VT. Inappropriate shocks are delivered due to a variety of reasons. Typically, atrial arrhythmias lead to an increase of ventricular contraction rate which is beyond the pre-set threshold value of the ICD algorithm. Among the rest of the popular roots of the problem

are sinus tachycardia, which is not fatal, supraventricular tachycardia (SVT), drug abuse, and ventricular oversensing. The latter is affected by a range of exogenic factors such as electromagnetic interference, possible ICD component malfunction (i.e., fractured lead), and endogenic factors such as T-wave oversensing. Inappropriate shocks worsen the patient's clinical condition of the patient resulting in higher mortality rates and an increase of stress levels, lowering the patient's quality of life.

1.5. Random Forest (RDF)

The integration of other sources of data such as perfusion data, and more complex electrogram data necessitates a more complex "discriminators". ICD algorithms are required to be of low computational complexity to meet power requirements, and to be clearly clinically explicable. Random decision forests (RDF) meet these two requirements.

RDF is a classification algorithm, which consists of decision trees. A hierarchical structure of "if-else" statements is known as a decision tree. The process starts from the root (top) of the tree and propagates to the end nodes (leaves)(Koehrsen, 2017). Depending on the input at each level of the structure certain outcomes are being ruled out, till a final decision is made.
A decision tree is the simplest form of a classifier. For each node of a decision tree classifier Gini importance is used as a decision-making mechanism. Gini importance $\sum_{i=1}^{C} f_i(1-f_i)$ is the frequency (f_i) of a single label (C number of distinct labels) at a specific node. In this project RDFs are used as implemented in ScikitLearn(Scikit-learn, n.d.).

In this implementation a decision tree calculates the importance of a node using Gini importance under the assumption that it is a binary tree (2 children) (Stacey Ronaghan, n.d.).The product of the weighted number of instances at node j with the impurity value of node j subtracted with the difference of the products of the impurity value of children nodes with the weighted instances at the children's nodes.

$$ni_j = w_j C_j - w_{right(j)} C_{right(j)} - w_{left(j)} C_{left(j)} \,. \quad (2)$$

The importance of each feature on a decision tree is estimated by dividing the sum of the feature importance of node *j* with the sum of the importance of all features:

$$fi_i = \frac{\sum_{j:node\ j\ splits\ on\ feature\ i} nij}{\sum_{k\in all\ nodes} nik} \,. \quad (3)$$

The importance of each feature on a decision tree is normalized (value between 0 and 1) by dividing it by the sum of all feature importance values:

$$normfi_i = \frac{fi^i}{\sum_{j\in all\ features} fij} \,. \quad (4)$$

Simply stated a decision forest is the collection of decision trees. Decision trees cooperate with each in a forest to achieve classification.
For each tree of the forest its importance value is calculated ($normfi_i$). These values are summed and divided by the number of the trees:

$$RFfi_i = \frac{\sum^{j\in all\ trees} normfiij}{T} \,. \quad (5)$$

Each tree process represents a classification model. The model with the best performance is defined as the prediction model (Stacey Ronaghan, n.d.)This algorithm offers a higher level of diversification.

2. Methods

This project focuses on developing an improved ICD arrhythmia detection algorithm that uses information from additional sensors that measure tissue blood flow, and more complex ECG analysis. To build upon existing ICDs re-implementing many of their underlying algorithms was needed, before adding our own work. Therefore, the project is divided into:

a) Basic signal acquisition and processing
b) The development of a cardiac activity detection algorithm (similar to current ICDs)
c) A basic arrhythmia detection algorithm (similar to current ICDs)
d) A perfusion signal interpretation algorithm (our proposed new addition).
e) A strategy for integrating perfusion information into the decision algorithm (new addition)
f) An integrated decision-making tool, including an RDF to decide upon intervention (new addition).

This project conceptualises the basis for improving their products based on the unmet needs of patients and their clinicians. The end-product of the project is a prototype establishing the incorporation of multiple sensors in an ICD. This project harnessed data collected by clinical members of the group from previous and current projects, and feeds into the device manufacturing project by other members of this research group. The data used in this project was collected under ethical approvals of the Health Research Authority (HRA) and the Health and Care Research Wales (HCRW).

This project required simultaneously collected electrical and laser Doppler perfusion data from patients under a variety of clinical and simulated conditions. Data was collected during

a) Sinus rhythm.
b) During spontaneously occurring ventricular tachycardia.
c) During simulated and induced ventricular arrhythmias at a variety of rates.
d) During simulated atrial arrhythmias at a variety of rates.
e) During simulated ventricular lead fracture.

2.1. Patient Data Collection

The data is collected and provided by specialized medical personnel on patients urgently admitted to the Heart Assessment Centre at Imperial College Healthcare NHS Trust, or from elective patients attending the cardiac devices clinic. Electrical and perfusion data collected during spontaneous heart rhythm disturbances resulted in no delay to the patient's treatment.

Patients had multiple non-invasive sensors placed over the skin including ECG electrodes and laser Doppler perfusion sensors. Patients either also had beat-by-beat blood pressure recorded from invasive catheters or non-invasive finger sensors (Figure 4). In addition, electrical recordings from ICD leads were acquired via the pacing system analyser.

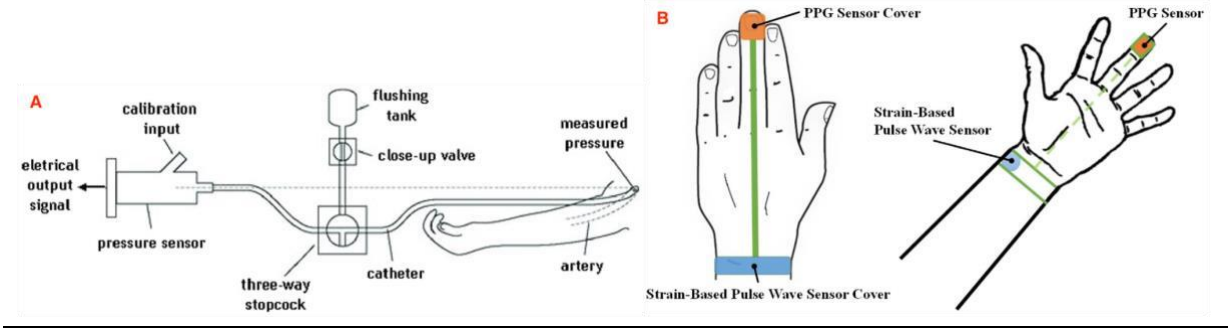

Figure 4: Blood pressure measuring techniques of (A)Invasive Catheter(Abreu, Carneiro & Restivo, 2020) (B)Non-invasive finger cuff(Wang *et al.*, 2018).

Analogue signals were converted to digital using a National Instrument digital acquisition device (1000Hz sampling, 12-bit) and stored as compressed CSVs.

For this project, the author developed the algorithms and software used to analyse the data.

Note that the invasive and non-invasive blood pressure was only used for validation purposes, as there are no sensors that could be safely implanted in the arterial system to provide such information to ICDs.

To ensure the integrity and privacy of each participant the collected data are pseudonymized and they are not associated with the participant's credentials. This fits under the project's objective of developing a non-discriminative device through the utilization of pseudonymized data. The data will be used to develop a cardiac activity detection algorithm as well as an arrhythmia detection algorithm.

2.2. Data Loading & Filtering

2.2.1 Data Loading

All the algorithms were designed with the ability to process information "live", i.e., the analysis would only be dependent on a small window of raw data, and that after this only recent identified features (such as RR interval or derived values) would be used.

Only a small buffer of 3 seconds of the recent raw data was kept and processed in 0.2 second increments. Derived parameters were stored in another buffer.

2.2.2 Filtering of ECG

As described in Section 1.2 an ECG signal is the recording of the action potentials from the cardiac muscles. This is achieved by placing electrodes either on the surface of the body (non-invasive) or inside the body(invasive). Both types are susceptible to artifacts, commonly known as noise. It is common for biological signals to suffer from noise, as shown in Figure 5 and Figure 6, therefore filtering was necessary. The raw ECG signal underwent low and then high pass filtering. The low pass filter (20 Hz, Butterworth) removed slow oscillations in the signal, such as those from patient movement, breathing, and electrode contact changes. The high pass filter (20 Hz, Butterworth) removes high-frequency noise such as line noise.

2.2.3 Filtering of laser Doppler Perfusion signal.

The raw laser Doppler perfusion device sensor signal is processed on the integrated device by a bandpass filter and then performing an FFT of the resultant signal. The energy within this signal is proportional to the velocity of blood within the tissue (He *et al.*, 2013). This signal is then output by the integrated device, and we record this as the raw perfusion signal. This signal is still noisy. It was observed that neither a low nor high pass filter were insufficient to filter out the artifacts. Therefore, a different approach was used, utilising a moving average sliding window over 100ms.

Once the artifacts had been removed from the signals the data were processed to extract statistical values that describe both the morphology of the signal and the physiological condition of the patient.

2.3. Development of Cardiac Activity Detection Algorithm

In this section the implementation of an "R-wave" ECG detector is dscribed. The algorithm comprises of two sub-systems, Section 2.3.1 describes the sub-division based on ECG signal and Section 2.3.2 describes the sub-systems based on Laser-Doppler signal. These two sections are in close cooperation. Essentially, both sub-systems extract meaningful statistical values which will be used as inputs of the learning paradigms. Before, any attempt is made on developing the systems, it is important to understand and establish a system that inputs and handles raw ECG and Laser-Doppler signals.

Essentially the ECG algorithm detects the QRS complexes and based on the information deduced the perfusion detector slices a part of the data and deduces further information related to the peripheral perfusion.

2.3.1 ECG R-wave detection

The pre-processing stage of the algorithm described in the previous section resulted in an ECG signal centred around 0V. R-wave spikes may be predominantly negative or positive. Then the signal was processed using a methodology similar to Pan-Tompkinson (Pan & Tompkins, 1985). The filtered ECG signal was then squared and a moving sum over 1ms was calculated. This convers the signal into effectively something that represents the amount of energy with all positive values. Simple local peak-detection was performed to identify candidate peaks. A decaying threshold (set at 200ms at a peak, and decaying by 1over time(ms)) was used to detect the next significant peak. These strategies help reduce the risk of detecting a T-wave as an R-wave. This phenomenon occurs when a T-wave is almost as high as the preceding R-wave making conventional algorithms mistakenly detect the T-wave as an R-wave.

Having detected all the R-waves within the 2000ms window buffer of ECG data further extraction of information occurs. Firstly, the time interval (RR interval) between the first (incoming) QRS complex and the following QRS complex. The RR interval is converted to beats per minute (bpm), by dividing it into 60000ms.

$$BPM = \frac{60{,}000}{rr\_interval} \tag{6}$$

Using the detected R-waves, the ECG was segmented into individual beats. For each RR interval a variety of statistical parameters were calculated from the electrical signal as a way of capturing morphological information and providing a statistical description. The mean, standard deviation, kurtosis, and skewness of the ECG signal were extracted. These features were later used in the Random Decision Forest algorithm.

2.3.2 PPG/Laser peaks detection

The laser Doppler perfusion signal (Figure 7) captures the phasic nature of the blood flow through the tissues. Whilst higher values indicate faster velocities, the units are arbitrary. Consequently, whilst the absolute value may provide some information, relative changes are likely to be more informative.

However, even then, the signal needs further processing. On even relatively short timescales the absolute value of the signal may change 10-fold resulting from movement of the sensor, tissue pressure (which compresses capillaries), and other sources of noise (Figure 7). However, one key observation is that the pulsatile nature of the signal remains.

Therefore, the perfusion signal was further processed by gating it using the detected R-waves from the ECG. Over a 6-beat window 'ensembled' the segmented portions of the perfusion signal to form a consensus(Keene *et al.*, 2019). The raw signal was pre-processed by taking its logarithm and subtracting out the mean before ensembling. This has the effect of transforming a measurement of the peak-to-peak height to a relative (log percentage) scale.

The advantages of this approach can be seen in Figure 8. In this figure the oscillations are visible but contaminated by large changes in the absolute value. After transforming the signal, segmenting, and ensembling a high-quality signal is obtained.

The QRS complex on the ECG signal precedes the perfusion peak recorded by the PPG. Therefore, when both signals are aligned it is observed that the perfusion peak comes some 100 to 200ms after the QRS complex is recorded (Figure 8). This delay in the laser-doppler signal is variable and depends on the BPM. The perfusion peak of the first QRS complex is going to be located between the first and the second QRS complexes, rr_interval. Therefore, by detecting the perfusion peak positioned in the specific time interval it is possible to deduce the time difference between the R-wave and the peak of the perfusion, which is used to appropriately shift the rr_interval by a few milliseconds. The new shifted interval is used to cut a window of the perfusion signal that accurately corresponds to its "mother" QRS complex. This extracted chunk the mean, standard deviation, kurtosis, and skewness are calculated providing a morphological description of the ECG signal.

It is key to segment the perfusion signal using the ECG signal to ensure that any oscillations have arisen from contraction of the heart rather than noise. If, for example, the oscillations in the perfusion signal arose from CPR, the match to the intrinsic electrical activity would be broken, and the system algorithm would correctly detect that the perfusion signal did not relate to the intrinsic electrical activity of the heart.

Due to that lag in the feedback of the perfusion of heart an uncertainty is generated about the physiological condition of the patient. Therefore, a record of the last six perfusion chunks is held, to produce a consensus of these signals. Utilizing the consensus curve the gradient, and amplitude of the normal curve as well as the amplitude of the logarithmic consensus curve are calculated. To determine the haemodynamic stability of the patient a comparison of the six perfusion curves takes place to determine the similarity of the perfusion curves and therefore establish whether or not the patient is haemodynamically stable.

$$similarity\ score_{datapoint(t)} = \sqrt{curve_1{}^2{}_{datapoint(t)} - curve_2{}^2{}_{datapoint(t)}} \quad (7)$$

For each perfusion curve a similarity score produced. The average of the similarity scores of the six curves is estimated and therefore a quality score of the last six haemodynamic instance is produced. In case the device is equipped with two laser doppler then similarity score would be used to determine which laser is going to be preferred. The similarity score captures the confidence in the quality of the signal.

2.2.3 Integration of the perfusion score into the decision-making algorithms

Other groups have attempted to utilise perfusion monitors as a surrogate for blood pressure (Mousavi *et al.*, 2019; Zhang & Feng, n.d.; Schlesinger *et al.*, 2020; Elgendi *et al.*, 2019; Anon, n.d.). These have been based on simple transformations of features (such as the time to peak) and statical strategies ranging from simple linear regression to large-scale convolution neural networks of the underlying perfusion signal. Various groups have claimed strong correlation between these features and the patients' blood pressure. In the project this relationship was assessed but such strong data were not found. An attempt to reconstruct a linear regression and machine learning approach using a SVM to derive the blood pressure(Zhang & Feng, n.d.; Mousavi *et al.*, 2019) was made, but again the results were not strong. The author did not proceed to neural network approaches, like Schlesinger *et al., as* they would exceed the power requirements of implantable devices such as ICDs. Therefore, the author was opted to integrate the derived features directly into the decision-making algorithm rather than try to approximate blood pressure.

By examining individually each feature extracted it was established that there was no clear correlation strong enough to be utilized for estimating the actual blood pressure, especially under non-normal conditions. However, these statistical features provided enough evidence to exploit a correlation with the patient's condition.

By combining information produced from the previous and this current section it is possible to produce a discriminant value determining the haemodynamic condition of the patient and whether they are undergoing a VT, AAI or VVI.

$$discriminant = \log_{10}(perfusion\ gradient * rr\_interval_2^{\frac{1}{2}} * simialrity\ score) \quad (4)$$

2.4. Development of decision-making tool including a random decision forest

The previous two sections derive insights for the physiological condition of a patient by analysing signals from both ECG and laser doppler sensors. Based on this beat-by-beat analysis an ICD has to decide whether or not the condition of the patient requires a shock-based treatment. For this purpose, two Random Forest classifiers (RDF) and a group of rules (if-else statements) were implemented. The data provided were also labelled by medical experts as two different sets of classes.

Two decision tools were developed.

a) Classification of the underlying rhythm into: normal sinus rhythm, noise, ventricular pacing, atrial pacing, and ventricular tachycardia.
b) Determination if a shock (or alternative electrical therapy) should be registered

The first set suggests the condition of the patient or the signal as Normal, Noise, simulated atrial tachycardia, simulated ventricular tachycardia, and clinical ventricular tachycardia.

These processes were designed to operate in a hierarchal strategy. If the first model determines that the signal is normal or just noise, then it did not proceed to the second process. If it was determined that it was neither of these two classes, it passed to the process for deciding if a shock (or no shock) was needed. The classifiers operated every 2000ms. The data was split into 60% for training, 30% for tuning, and 10% for internal validation (Tan *et al.*, 2014)(Figure 4).

The optimized parameters for each RDF model are number of features per split (n_estimators), the maximum number of features when looking for a split (max_features), and the tree's length (max_depth). Both n_estimators and max_depth are numerically continuous parameters, and an automatic search is set for values between 200 and 2000 for n_estimators and values between 100 and 500 max_depth. Models that achieved more than 80% of accuracy would be saved and trained on the whole 90% of the original dataset and saved again. For both models the most optimal set of parameters was max_depth=300, max_features= auto, n_estimators= 600.

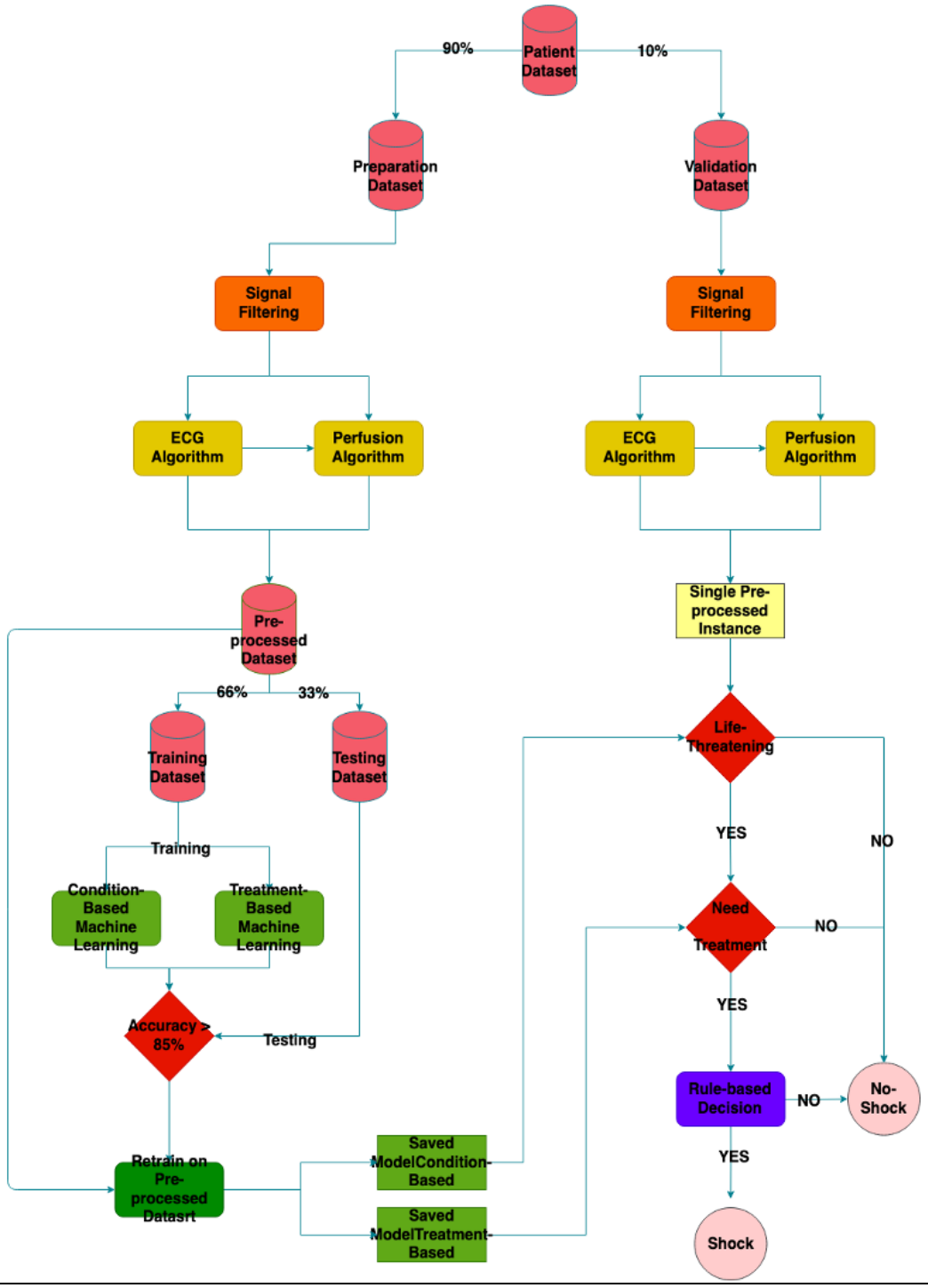

Figure 5: Flow chart of the training, testing and decision-making mechanism

As RDFs cannot include biased weights on their inputs (i.e. assign a high weight to a very informative feature), it was hypothesised that adding in a final decision process using the perfusion discriminant feature, would resolve this issue. The final decision for inclusion of the perfusion discriminant into the algorithm was as follows.

If the RDF decision was Shock and the discriminant was negative (i.e. poor perfusion) then a shock was indicated. Similarly, if the RDF decision was no-shock and the discriminant was positive (i.e. good perfusion) then no-shock was suggested.

If there was a discrepancy between the RDF and the perfusion discriminant then the algorithm shown in Figure 5 was used. In Figure 6 the perfusion discriminant-based rules that were incorporated alongside the final RDF model are displayed in a pseudo-code format.

```
if suggested_treatment == "Shock" and perfusion discriminant>0:
    final_treatment="Shock"
elif suggested_treatment == "No Shock" and perfusion discriminant <0:
    final_treatment = "No Shock"
elif treament == "Shock" and perfusion discriminant <0:
    probability of Shock=ml_prob[0][1]*-1
    if absolute(probability of Shock) > 0.8:
        probability of Shock = probability of Shock *2
    else:
        probability of Shock = probability of Shock *1.5
    temporary treatment = perfusion discriminant + probability of Shock
    if temporary treatment <0:
        final_treatment="Shock"
    else:
        final_treatment="No Shock"
elif suggested_treatment == "No Shock" and perfusion discriminant >0:
    if absolute(perfusion discriminant) > 1.5:
        perfusion discriminant = 2.5* perfusion discriminant
    probability of No Shock = ml_prob[0][0]*2
    temporary treatment = perfusion discriminant + probability of No Shock
    if temporary treatment <0:
        final_treatment="Shock"
    else:
        final_treatment= "No Shock"
```

Figure 6: Pseudo-code for the incorporation of RDF with the rule-based decision-making mechanism

3. Results

3.1. Data

The obtained datasets from patients represented minutes/ hours of recordings. A single medical reviewer classified them into needing a shock or no-shock based on access to all data including the invasive and noninvasive blood pressure. The breakdown of the classifications is shown in Figure 7.

Patient	Experiment	File	Period	Begin	End	ECG	BP	Laser1	Laser2	Rhythm	BP	HRS
VTFI0002	Exp1	VTFI0002_30_06_2020_112536_VVI160_LAD.zip	Baseline	0	16700	BP	bpao	plethh		No Shock	No Shock	No Shock
VTFI0002	Exp2	VTFI0002_30_06_2020_112536_VVI160_LAD.zip	VVI 160	16700	51400	BP	bpao	plethh		Shock	No Shock	No Shock
VTFI0002	Exp3	VTFI0002_30_06_2020_112536_VVI160_LAD.zip	Baseline	51400	86000	BP	bpao	plethh		No Shock	No Shock	No Shock
VTFI0002	Exp4	VTFI0002_30_06_2020_112711_VVI140_LAD.zip	Baseline	0	29400	BP	bpao	plethh		No Shock	No Shock	No Shock
VTFI0002	Exp5	VTFI0002_30_06_2020_112711_VVI140_LAD.zip	VVI 140	29400	60000	BP	bpao	plethh		Shock	No Shock	No Shock
VTFI0002	Exp6	VTFI0002_30_06_2020_112711_VVI140_LAD.zip	Baseline	60000	108000	BP	bpao	plethh		No Shock	No Shock	No Shock
VTFI0002	Exp7	VTFI0002_30_06_2020_112905_VVI180_LAD.zip	Baseline	0	25500	BP	bpao	plethh		No Shock	No Shock	No Shock
VTFI0002	Exp8	VTFI0002_30_06_2020_112905_VVI180_LAD.zip	VVI 180	25500	68000	BP	bpao	plethh		Shock	No Shock	Borderline
VTFI0002	Exp9	VTFI0002_30_06_2020_112905_VVI180_LAD.zip	Baseline	68000	102000	BP	bpao	plethh		No Shock	No Shock	No Shock
VTFI0002	Exp10	VTFI0002_30_06_2020_113240_VVI180_LAD.zip	Baseline	0	15500	BP	bpao	plethh		No Shock	No Shock	No Shock
VTFI0002	Exp11	VTFI0002_30_06_2020_113240_VVI180_LAD.zip	VVI 180	15500	59300	BP	bpao	plethh		Shock	No Shock	Borderline
VTFI0002	Exp12	VTFI0002_30_06_2020_113240_VVI180_LAD.zip	Baseline	59300	103000	BP	bpao	plethh		No Shock	No Shock	No Shock
VTFI0002	Exp13	VTFI0002_30_06_2020_113429_VVI120_LAD.zip	Baseline	0	29300	BP	bpao	plethh		No Shock	No Shock	No Shock
VTFI0002	Exp14	VTFI0002_30_06_2020_113429_VVI120_LAD.zip	VVI 120	29300	75900	BP	bpao	plethh		Shock	No Shock	No Shock
VTFI0002	Exp15	VTFI0002_30_06_2020_113429_VVI120_LAD.zip	Baseline	75900	110000	BP	bpao	plethh		No Shock	No Shock	No Shock
VTFI0002	Exp16	VTFI0002_30_06_2020_113625_VVI180_LAD.zip	Baseline	0	27000	BP	bpao	plethh		No Shock	No Shock	No Shock

Figure 7: Example of patients' recordings with classification suggestions

3.1.1 Signal Filtering

The raw ECG signals were underwent low-pass then high-pass filtering (sample period = 1, sample rate = 1000 Hz, low-cut = 500Hz, high-cut=750 Hz, cutoff frequency = 20Hz, Nyquist Frequency=500Hz, number of samples = 1000, cubic sinusoidal function for approximating the wave), which successfully smoothens the signal and substantially decreases both the electrical and movement based noise(Figure 8A).

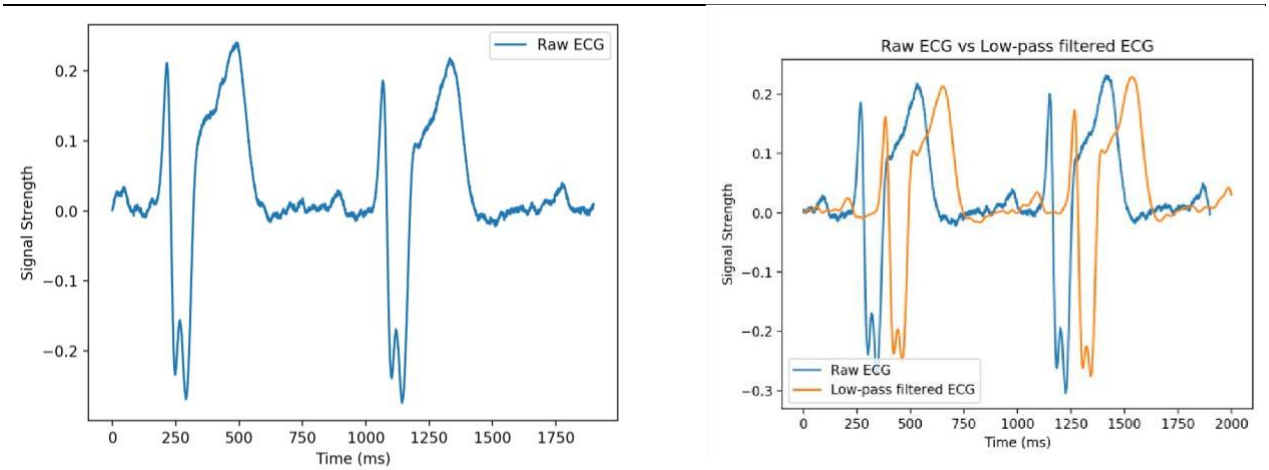

Figure 8: (A) Raw ECG signal. (B) Raw vs Low-pass filtered ECG signal

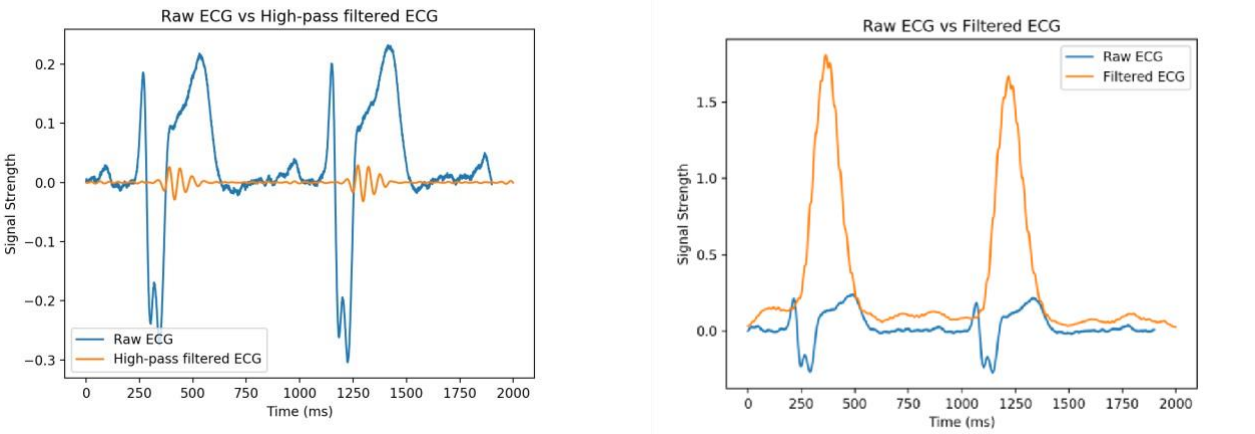

Figure 9: ECG signal(A) Raw vs High-pass filtered (B) Raw vs Filtered

The ECG signal was then squared, and a moving window of 100ms that summated the signal (Figure 9B).

The perfusion signal derived by the device from the raw laser sensor had a substantial amount of high frequency noise. It was found that a similar band-pass technique was not effective, and a high-pass filter would remove the somewhat important average value. Therefore, a moving average over a 100ms window was used. This technique allowed the removal of noise by averaging the signal's input and by highlighting the true signal (Figure 10).

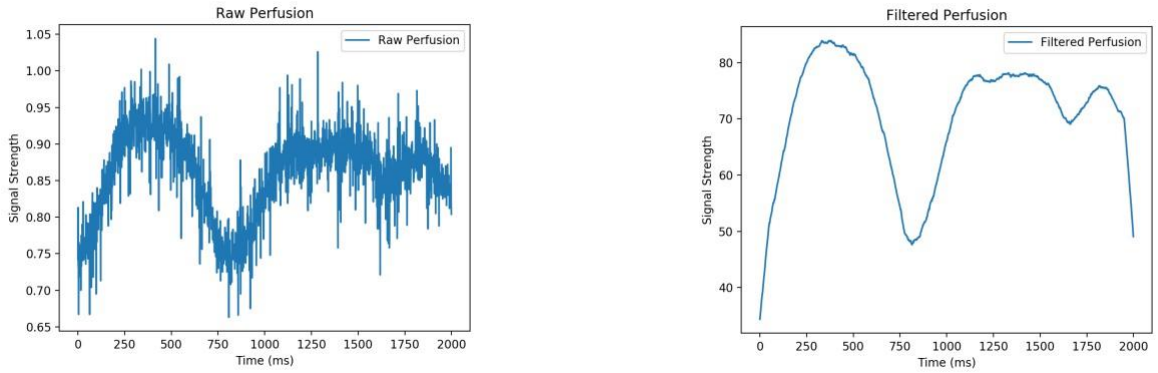

Figure 10: Raw perfusion signal and filtered perfusion signal

3.2. Cardiac activity detection and generation of the 6-beat perfusion consensus signal

Figure 11 shows the "live" processing of a set of signals during simulated VT at 180 BPM. Typically, such a fast VT would be shocked by currently devices based on the rate. The raw ECG signal is shown in panel A with the pacing spikes evident. The filtered, rectified, and integrated signal is shown in panel B with the R-wave detector shown. The relatively noisy PPG perfusion signal is shown in panel C (red). The successive R-R intervals are used to segment the perfusion signal. The previously beats smoothed and segmented beat is shown in panel D. The preceding 6 beats are shown in panel E with their consensus in panel F. A clear a strong consensus signal on the perfusion trace indicates that the patient, despite being in a simulated VT with a rapid rate was tolerating it. At the time their BP was 120mmHg.

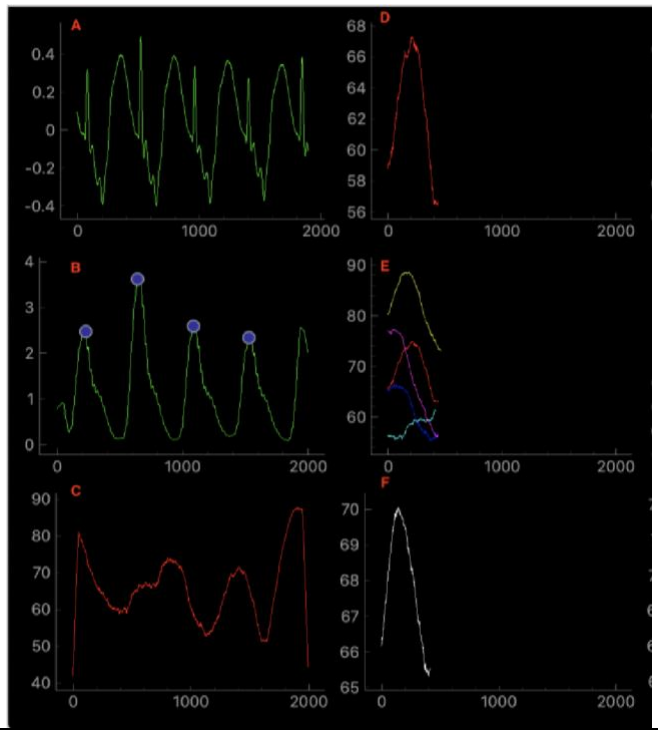

Figure 11: Example during simulated VT. (A) Raw ECG (green)(B) Filtered ECG (green)(C) Perfusion signal(red) (PPG sensor 1) (D) Current perfusion cut (red) (PPG sensor 1) (E) Current and

five previous perfusion cuts (multicolour) (PPG sensor 1) (F) Consensus of the perfusion signal (white) (PPG sensor 1)

3.3. Extraction of Statistical Values

From the segmented ECG and perfusion signals, a variety of statistical parameters are calculated for each beat to use as features for the RDF classifier. An example of the ECG and PPG extracted features for three successive beats is shown in Figure 12. The values for these features throughout a single recording are shown in Figure 12. Whilst there are clear patterns amongst the values, it is clear that a single parameter is not enough, and a decision-making tool is needed.

A: ECG extracted values

BPM	EGM Mean RV	EGM STD RV	EGM Skewness RV	EGM Kurtosis RV	EGM Quality	R-R Interval RV
78.2268579	0.52683931	0.677372566	1.408372142	0.484423396	0.857545532	767
78.3289817	0.480122249	0.652159671	1.50509257	0.760847663	1.271034343	766
78.6369594	0.466595772	0.642671227	1.475936666	0.708805877	1.341404246	763

B: LDF extracted values

BP Estimat	Per Mean	Per STD	Per Skewness	Per Kurtosis	Current Perfusion Grad	Quality of Perfusion	Perfusion Amplitude	Magic Laser
-0.358840485	73.7078749	6.59232554	-0.333780386	-0.912129265	0.326772973	0.713107292	1.718759544	-17.18759544
-0.541576235	73.3947134	7.61544754	-0.31334072	-1.254179602	0.562282793	0.632870938	1.090292028	-10.90292028
-0.496568587	73.9422914	7.03108307	-0.344092347	-1.259527886	0.57014274	0.567135931	1.340353562	-13.40353562

Figure 12: Example of statistical values extracted by ECG(A) and PPG(B) signals

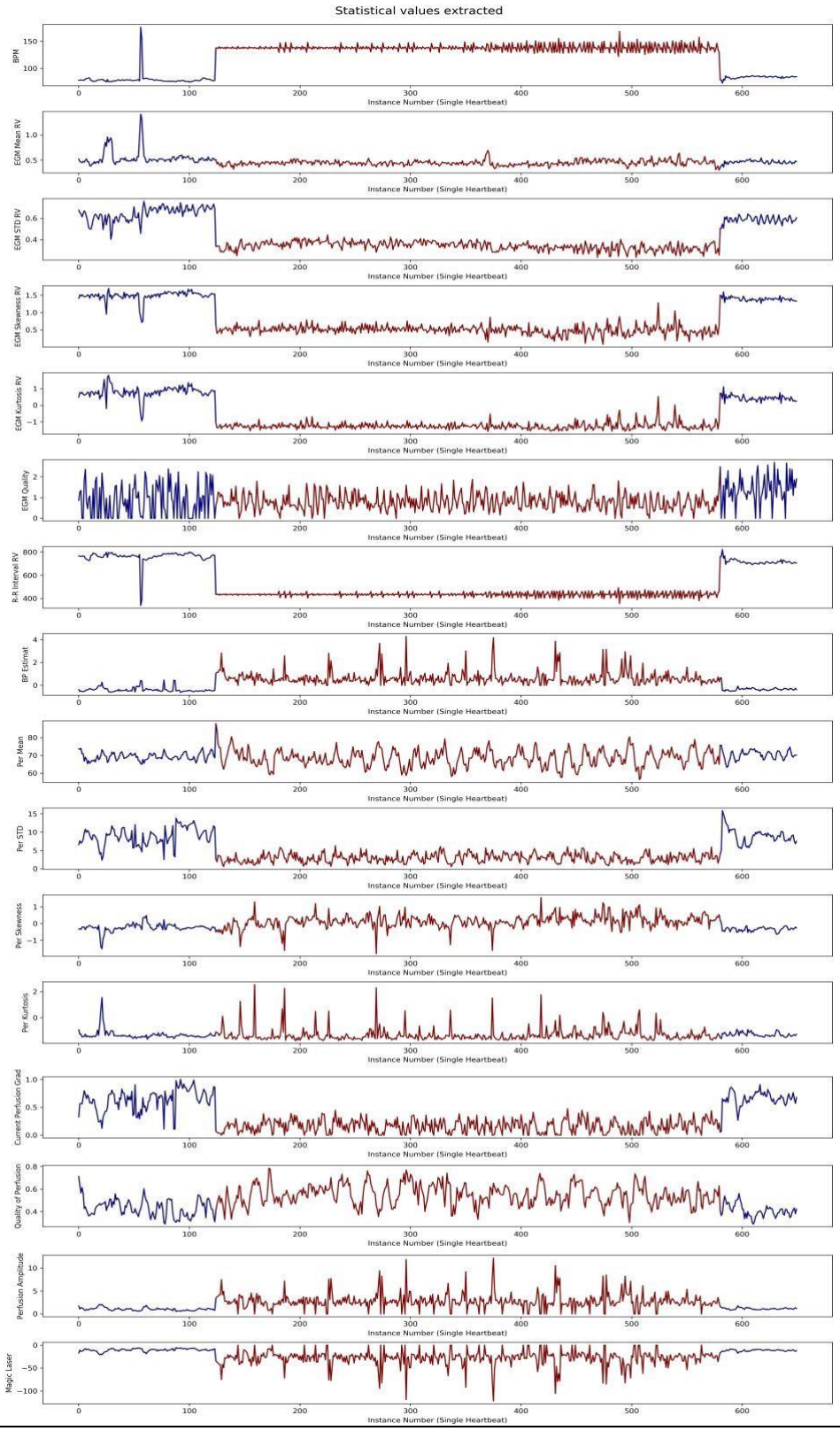

Figure 13: Statistical values extracted from ECG and PPG over a beat-by-beat analysis

3.4. Decision making

3.4.1. Trace Classification

Table 1 shows the confusion matrix for the condition-based trace classifier. Simulated VT and Clinical VT were classified separately, to determine if the subsequent Shock/ No- Shock classifier was not biased to the simulated situation.

When considering potentially shockable rhythms – Normal, noise, and simulated SVT against VT, the RBF had an sensitivity towards VT, and accuracy levels of 83.2%.

Table 1: Confusion matrix of condition-based Random Forest

True/Predicted	Noise	Normal	VVI	AAI	VT
Noise	181	54	1	2	39
Normal	20	1433	0	3	411
Simulated VT	2	1	301	7	78
Simulated SVT	0	31	9	102	82
Clinical VT	6	51	51	3	2391

3.4.2. Shock / No shock classification

Two strategies were tested. Firstly, using the RDF alone without the addition of the final perfusion discriminant algorithm, and then with. As discussed in Section 2.4 this was added as in some occasions the RDF is unable to confidently determine if the instance is shock/ no shock. Without this addition the performance of the decision-making mechanism was good (Table 2). The models were a bit more sensitive with No Shock instances and it achieved accuracy levels of 89.5%.

Table 2: Confusion matrix of treatment-based Random Forest

True/Predicted	Shock	No-Shock
Shock	2203	440
No-Shock	2	1760

Combining the RBF with the perfusion discriminant-based conditions significantly increased the accuracy level of the decision-making mechanism reached 97.46%

Table 3: Confusion matrix of treatment-based Random Forest with the rulebased decision-making mechanism

True/Predicted	Shock	No-Shock
Shock	7184	209
No-Shock	133	5877

4. Discussion

The quality of the product of Section 2.2 can be assessed by the end result, which is significant. Having properly pre-processed and cleaned data signals is the basis for developing a reliable and accurate algorithm.

In Section 3.2 it is evident that the algorithm is capable of recognizing more than one QRS complexes with a relative ease. And therefore, the extracted statistical ECG values are closer to representing the actual morphological and physiological condition of both the signal and the patient. That can be seen by the accuracy score achieved by the condition-based RDF (83.2%) whereas the score achieved by the treatmentbased model reaches a whopping 89.5%.

The percentage gap noticed on the model's accuracy levels is rational, since the condition-based model has more classes to select from. Therefore, it is more likely instances to be similar to each other, morphologically, but belonging to different labels. From the confusion matrix somebody can notice that the highest misclassification occurred for Simulated SVT and Simulated VT classes. Instances of these classes were classified mostly as Clinical VT, indicating that these conditions might be morphologically and physiologically similar. Instances that were classified as Simulated SVT, Simulated VT and clinical VT would be further processed by the second RDF, suggesting an appropriate treatment.

If there was not a second RDF in place the percentage of inappropriate shocks would have reached 19.71% of the total test cases. However, as shown in the confusion matrix of the treatment-based model approximately 16.47% of Shock instances were misclassified as No-Shock, as they were not conclusive enough. Meaning that 16.47% of Shock needed cases would not be treated. The model misclassified only two instances of No-Shock as Shock instances, minimizing the number of inappropriate shocks.

When the rule-based decision-making mechanism was implemented alongside the two RDFs the algorithm treated cases with 97.46% accuracy. Meaning that even less instances were misclassified, decreasing the chances of registering an inappropriate treatment. Taking a deeper look into the misclassified cases it is possible to deduce that only 133 out of the 13403 instances were inappropriately treated cases, which is less than 1%. While the rest of the misclassified cases in their majority were Shock instances and they were predicted as No Shock treatment, but the perfusion discriminant suggested that the haemodynamic condition of the patient was stable enough. Therefore, setting the current state of the patient as non-life threatening. With current conventional ICD the number of inappropriate treatments is approximately 18.5% due to the lack of utilization of PPG data.

5. Conclusion

The project's aim was the implementation of extra senor data (PPG) to help diagnose the condition of a patient an ICD. To achieve this, extraction of extraction of statistical features from both the ECG and PPG signals was critical. The information derived by the cardiac activity detection algorithm was used as part of the perfusion detection mechanism resulting to the complete extraction of such features.

The decision-making mechanism achieved a real-time on the fly classification of patients' instances with accuracy levels of 97.46%, only when the perfusion discriminant was incorporated as part of the rulebased mechanism. This, not only proves the importance of implementing PPG sensors on an ICD but also the contribution of this paper with establishing a new biomarker. Overall, the project was able to treat 97.46% of the cases correctly, significantly decreasing the inappropriate treatments overall to 2.54%. Whereas the total of inappropriate shock registered by the suggested algorithm was brough to a minimal 1% as opposed to 18.5% of inappropriate treatments registered on average by conventional devices. The main objective of the project to provide a means of improving the quality of living for patients with an ICD was also achieved.

5.1. Future Outlook

The promising results of the project, set the basis for future investigation of the importance of PPG data when deciding the condition of a patient. In addition, it provides proof of concept for implementing such sensors on conventional ICDs to be further tested for its feasibility and reliability.

6. References

Abreu, P., Carneiro, F. & Restivo, M.T. (2020) Screening system for cardiac problems through noninvasive identification of blood pressurewaveform. *Information (Switzerland)*. [Online] 11 (3). Available from: doi:10.3390/INFO11030150.

Aguilera, A.L., Volokhina, Y. V. & Fisher, K.L. (2011) Radiography of Cardiac Conduction Devices: A Comprehensive Review. *RadioGraphics*. [Online] 31 (6), 1669–1682. Available from: doi:10.1148/rg.316115529 [Accessed: 28 February 2021].

Anon (n.d.) *Samsung and UCSF Introduce My BP Lab, a Smartphone App for Blood Pressure and Stress Research | UC San Francisco*. [Online]. Available from: https://www.ucsf.edu/news/2018/02/409911/samsung-and-ucsf-introduce-my-bp-lab-smartphoneapp-blood-pressure-and-stress [Accessed: 7 September 2021].

Davey, P. & Sharman, D. (2018) The electrocardiogram. *Medicine*. [Online] 46 (8), 443–452. Available from: doi:10.1016/j.mpmed.2018.05.004.

Elgendi, M., Fletcher, R., Liang, Y., Howard, N., et al. (2019) The use of photoplethysmography for assessing hypertension. *npj Digital Medicine*. [Online] 2 (1). Available from: doi:10.1038/S41746019-0136-7.

He, D., Nguyen, H.C., Hayes-Gill, B.R., Zhu, Y., et al. (2013) Laser Doppler Blood Flow Imaging Using a CMOS Imaging Sensor with On-Chip Signal Processing. *Sensors (Basel, Switzerland)*. [Online] 13 (9), 12632. Available from: doi:10.3390/S130912632 [Accessed: 8 September 2021].

Helton, M.R. (2015) Diagnosis and management of common types of supraventricular tachycardia. *American Family Physician*. [Online] 92 (9), 793–800. Available from: www.aafp.org/afp. [Accessed: 28 February 2021].

Johns Hopkins Medicine (2020) *Ventricular Tachycardia | Johns Hopkins Medicine*. [Online]. 2020. Johns Hopkins Medicine. Available from: https://www.hopkinsmedicine.org/health/conditions-anddiseases/ventricular-tachycardia [Accessed: 11 February 2021].

Keene, D., Shun-Shin, M.J., Arnold, A.D., Howard, J.P., et al. (2019) Quantification of Electromechanical Coupling to Prevent Inappropriate Implantable Cardioverter-Defibrillator Shocks. *JACC: Clinical Electrophysiology*. [Online] 5 (6), 705–715. Available from: doi:10.1016/j.jacep.2019.01.025 [Accessed: 19 February 2021].

Koehrsen, W. (2017) *Random Forest Simple Explanation. Understanding the Random Forest with an… | by Will Koehrsen | Medium*. [Online]. 2017. Available from: https://williamkoehrsen.medium.com/random-forest-simple-explanation-377895a60d2d [Accessed: 7 September 2021].

Medicine, J.H. (2020) *Ventricular Fibrillation | Johns Hopkins Medicine*. [Online]. 2020. Johns Hopkins Medicine. Available from: https://www.hopkinsmedicine.org/health/conditions-anddiseases/ventricular-fibrillation [Accessed: 28 February 2021].

Mousavi, S.S., Firouzmand, M., Charmi, M., Hemmati, M., et al. (2019) Blood pressure estimation from appropriate and inappropriate PPG signals using A whole-based method. *Biomedical Signal Processing and Control*. [Online] 47, 196–206. Available from: doi:10.1016/j.bspc.2018.08.022.

Pan, J. & Tompkins, W.J. (1985) A Real-Time QRS Detection Algorithm. *IEEE Transactions on Biomedical Engineering*. [Online] BME-32 (3), 230–236. Available from: doi:10.1109/TBME.1985.325532.

Patrick Mullins, M. (2016) *Scholar Commons Automated Device to Measure Slurry Properties in Drilled Shafts*. [Online] Available from: http://scholarcommons.usf.edu/etdhttp://scholarcommons.usf.edu/etd/6333 [Accessed: 8 September 2021].

Peyrol, M., Barraud, J., Cautela, J., Maille, B., et al. (2017) Controlled sedation with midazolam and analgesia with nalbuphine to alleviate pain in patients undergoing subcutaneous implantable cardioverter

defibrillator implantation. *Journal of Interventional Cardiac Electrophysiology*. [Online] 49 (2), 191–196. Available from: doi:10.1007/S10840-017-0255-5.

Van Rees, J.B., Borleffs, C.J.W., De Bie, M.K., Stijnen, T., et al. (2011) Inappropriate implantable cardioverter-defibrillator shocks: Incidence, predictors, and impact on mortality. *Journal of the American College of Cardiology*. [Online] 57 (5), 556–562. Available from: doi:10.1016/j.jacc.2010.06.059 [Accessed: 7 September 2021].

Schlesinger, O., Vigderhouse, N., Eytan, D. & Moshe, Y. (2020) Blood Pressure Estimation from PPG Signals Using Convolutional Neural Networks and Siamese Network. In: *ICASSP, IEEE International Conference on Acoustics, Speech and Signal Processing - Proceedings*. [Online]. 1 May 2020 Institute of Electrical and Electronics Engineers Inc. pp. 1135–1139. Available from: doi:10.1109/ICASSP40776.2020.9053446.

Scikit-learn (n.d.) *scikit-learn: machine learning in Python — scikit-learn 0.24.2 documentation*. [Online]. Available from: https://scikit-learn.org/stable/ [Accessed: 7 September 2021].

Stacey Ronaghan (n.d.) *The Mathematics of Decision Trees, Random Forest and Feature Importance in Scikit-learn and Spark | by Stacey Ronaghan | Towards Data Science*. [Online]. Available from: https://towardsdatascience.com/the-mathematics-of-decision-trees-random-forest-and-featureimportance-in-scikit-learn-and-spark-f2861df67e3 [Accessed: 7 September 2021].

Tamura, T. (2014) Blood Flow Measurement. *Comprehensive Biomedical Physics*. [Online] 5, 91–105. Available from: doi:10.1016/B978-0-444-53632-7.00511-6.

Tan, P.N., Steinbach, M., Kumar, V. & al., undefined et (2014) *Introduction to Data Mining, First Edition*. [Online] (September), undefined-undefined. Available from: https://www.mendeley.com/catalogue/8b946cb9-cd5e-35cb-b9f5-a3aa41cce0c1/ [Accessed: 7 September 2021].

Thompson-Nauman,Amy E. ; Christie,Melissa G.T. ; Degroot,Paul J. ; Dolan, B.L. (2014) *Implantable cardioverter-defibrillator (icd) system including substernal lead*. [Online]. Available from: https://patents.google.com/patent/US20140330327A1/en [Accessed: 7 February 2021].

Wang, Y.-J., Chen, C.-H., Sue, C.-Y., Lu, W.-H., et al. (2018) Estimation of Blood Pressure in the Radial Artery Using Strain-Based Pulse Wave and Photoplethysmography Sensors. *Micromachines 2018, Vol. 9, Page 556*. [Online] 9 (11), 556. Available from: doi:10.3390/MI9110556 [Accessed: 8 September 2021].

Ward,Jeremy P. T. ; Linden, R.W.A. (2017) *Physiology at a Glance*. 4th edition. [Online]. John Wiley & Sons, Incorporated. Available from: https://ebookcentral.proquest.com/lib/imperial/reader.action?docID=4816495 [Accessed: 19 February 2021].

Wiggers, C.J. (1940) The mechanism and nature of ventricular fibrillation. *American Heart Journal*. [Online] 20 (4), 399–412. Available from: doi:10.1016/S0002-8703(40)90874-2.

World Health Organization (2018) *WHO - The top 10 causes of death*. [Online]. 2018. 24 Maggio. Available from: https://www.who.int/news-room/fact-sheets/detail/the-top-10-causes-of-death [Accessed: 13 February 2021].

Zhang, Y. & Feng, Z. (n.d.) A SVM Method for Continuous Blood Pressure Estimation from a PPG Signal. *Proceedings of the 9th International Conference on Machine Learning and Computing*. [Online] Available from: doi:10.1145/3055635 [Accessed: 7 September 2021].